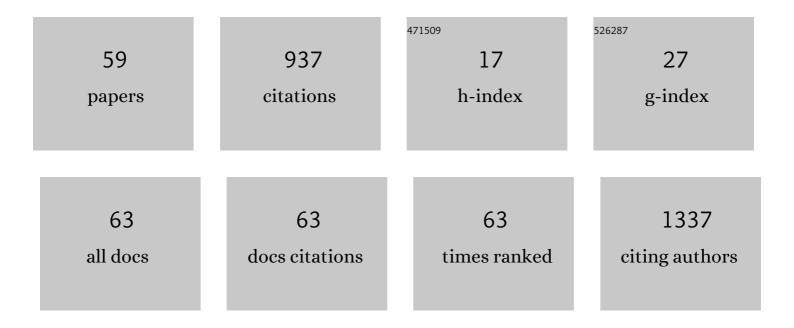
List of Publications by Year in descending order

Source: https://exaly.com/author-pdf/7823222/publications.pdf Version: 2024-02-01



#	Article	IF	CITATIONS
1	Deep regression using 99mTc-DTPA dynamic renal imaging for automatic calculation of the glomerular filtration rate. European Radiology, 2023, 33, 34-42.	4.5	2
2	Fusing deep and handcrafted features for intelligent recognition of uptake patterns on thyroid scintigraphy. Knowledge-Based Systems, 2022, 236, 107531.	7.1	3
3	Synthesis, radiolabeling, and evaluation of a potent β-site APP cleaving enzyme (BACE1) inhibitor for PET imaging of BACE1 in vivo. Bioorganic and Medicinal Chemistry Letters, 2022, 59, 128543.	2.2	3
4	An automatic fine-grained skeleton segmentation method for whole-body bone scintigraphy using atlas-based registration. International Journal of Computer Assisted Radiology and Surgery, 2022, 17, 673-681.	2.8	0
5	A novel theranostic probe [ <sup>111</sup> In]In-DO3A-NHS-nimotuzumab in glioma xenograft. Radiochimica Acta, 2022, .	1.2	0
6	PET imaging of VEGFR and integrins in glioma tumor xenografts using 89Zr labelled heterodimeric peptide. Bioorganic and Medicinal Chemistry, 2022, 59, 116677.	3.0	8
7	Cross-granularity multi-task network for ischemia diagnosis and defect detection in the myocardial perfusion imaging. Knowledge-Based Systems, 2022, , 108877.	7.1	0
8	Carbon dot/inorganic nanomaterial composites. Journal of Materials Chemistry A, 2022, 10, 14709-14731.	10.3	42
9	A Brief Introduction to Porphyrin Compounds used in Tumor Imaging and Therapies. Mini-Reviews in Medicinal Chemistry, 2021, 21, 1303-1313.	2.4	4
10	The effect of hypothyroidism on referential background metabolic activity on 18F-FDG PET/CT. Quantitative Imaging in Medicine and Surgery, 2021, 11, 3666-3676.	2.0	3
11	Retro-enantio isomer of angiopep-2 assists nanoprobes across the blood-brain barrier for targeted magnetic resonance/fluorescence imaging of glioblastoma. Signal Transduction and Targeted Therapy, 2021, 6, 309.	17.1	31
12	Automatic identification of suspicious bone metastatic lesions in bone scintigraphy using convolutional neural network. BMC Medical Imaging, 2021, 21, 131.	2.7	11
13	A merged method for targeted analysis of amino acids and derivatives using parallel reaction monitoring combined with untargeted profiling by HILIC-Q-Orbitrap HRMS. Journal of Pharmaceutical and Biomedical Analysis, 2021, 203, 114208.	2.8	6
14	Synthesis and Preliminary Evaluation of <sup>131</sup> I-Labeled FAPI Tracers for Cancer Theranostics. Molecular Pharmaceutics, 2021, 18, 4179-4187.	4.6	31
15	Automatic differentiation of thyroid scintigram by deep convolutional neural network: a dual center study. BMC Medical Imaging, 2021, 21, 179.	2.7	7
16	Advanced Imaging Techniques for Differentiating Pseudoprogression and Tumor Recurrence After Immunotherapy for Glioblastoma. Frontiers in Immunology, 2021, 12, 790674.	4.8	14
17	F0F1-ATPase Contributes to the Fluoride Tolerance and Cariogenicity of Streptococcus mutans. Frontiers in Microbiology, 2021, 12, 777504.	3.5	5
18	Deep neural network based artificial intelligence assisted diagnosis of bone scintigraphy for cancer bone metastasis. Scientific Reports, 2020, 10, 17046.	3.3	45

#	Article	IF	CITATIONS
19	Automated diagnosis of bone metastasis based on multi-view bone scans using attention-augmented deep neural networks. Medical Image Analysis, 2020, 65, 101784.	11.6	43
20	New Frontiers in Molecular Imaging Using Peptide-Based Radiopharmaceuticals for Prostate Cancer. Frontiers in Chemistry, 2020, 8, 583309.	3.6	13
21	Biodegradable <sup>131</sup> Iodine‣abeled Microspheres: Potential Transarterial Radioembolization Biomaterial for Primary Hepatocellular Carcinoma Treatment. Advanced Healthcare Materials, 2020, 9, e2000028.	7.6	15
22	64Cu-labeled melanin nanoparticles for PET/CT and radionuclide therapy of tumor. Nanomedicine: Nanotechnology, Biology, and Medicine, 2020, 29, 102248.	3.3	16
23	Use of Tregs as a cellâ€based therapy via CD39 for benign prostate hyperplasia with inflammation. Journal of Cellular and Molecular Medicine, 2020, 24, 5082-5096.	3.6	9
24	Decreased striatal vesicular monoamine transporter 2 (VMAT2) expression in a type 1 diabetic rat model: A longitudinal study using micro-PET/CT. Nuclear Medicine and Biology, 2020, 82-83, 89-95.	0.6	6
25	<p>Bombesin-functionalized superparamagnetic iron oxide nanoparticles for dual-modality MR/NIRFI in mouse models of breast cancer</p> . International Journal of Nanomedicine, 2019, Volume 14, 6721-6732.	6.7	17
26	EFFECTIVE RADIATION DOSE OF 18F-FDG PET/CT: HOW MUCH DOES DIAGNOSTIC CT CONTRIBUTE?. Radiation Protection Dosimetry, 2019, 187, 183-190.	0.8	34
27	Positron Emission Tomography Imaging of Platelet-Derived Growth Factor Receptor Î <sup>2</sup> in Colorectal Tumor Xenograft Using Zirconium-89 Labeled Dimeric Affibody Molecule. Molecular Pharmaceutics, 2019, 16, 1950-1957.	4.6	16
28	Recent Advances in Prostate-Specific Membrane Antigen-Based Radiopharmaceuticals. Current Topics in Medicinal Chemistry, 2019, 19, 33-56.	2.1	13
29	Small Molecule Natural Products and Alzheimer's Disease. Current Topics in Medicinal Chemistry, 2019, 19, 187-204.	2.1	23
30	Radionuclide imaging and therapy in malignant melanoma after survivin promoter-directed sodium iodide symporter gene transfer in vitro and in vivo. International Journal of Clinical and Experimental Pathology, 2019, 12, 613-618.	0.5	1
31	Evaluation of astatine-211-labeled octreotide as a potential radiotherapeutic agent for NSCLC treatment. Bioorganic and Medicinal Chemistry, 2018, 26, 1086-1091.	3.0	16
32	Bombesin functionalized <sup>64</sup> Cu-copper sulfide nanoparticles for targeted imaging of orthotopic prostate cancer. Nanomedicine, 2018, 13, 1695-1705.	3.3	23
33	Quantification of radioactivity by planar gamma-camera images, a promoted method of absorbed dose in the thyroid after iodine-131 treatment. Scientific Reports, 2018, 8, 10167.	3.3	3
34	Endogenous IgG-based affinity-controlled release of TRAIL exerts superior antitumor effects. Theranostics, 2018, 8, 2459-2476.	10.0	19
35	Anti-prostate cancer activity of 8-hydroxyquinoline-2-carboxaldehyde-thiosemicarbazide copper complexes in vivo by bioluminescence imaging. Journal of Biological Inorganic Chemistry, 2018, 23, 949-956.	2.6	16
36	Rapid diagnosis of cisplatin-sensitive and resistant cervical squamous cell carcinomas by reverse transcription loop-mediated isothermal amplification. International Journal of Clinical and Experimental Pathology, 2018, 11, 882-887.	0.5	0

#	Article	IF	CITATIONS
37	Improved radioiodine-131 imaging of prostatic carcinoma using the sodium iodide symporter gene under control of the survivin promoter. International Journal of Clinical and Experimental Pathology, 2018, 11, 4067-4072.	0.5	0
38	Cotransfecting norepinephrine transporter and vesicular monoamine transporter 2 genes for increased retention of metaiodobenzylguanidine labeled with iodine 131 in malignant hepatocarcinoma cells. Frontiers of Medicine, 2017, 11, 120-128.	3.4	1
39	Targeted Imaging of Tumor-Associated Macrophages by Cyanine 7-Labeled Mannose in Xenograft Tumors. Molecular Imaging, 2017, 16, 153601211668949.	1.4	26
40	CuCl PET/CT imaging of mouse muscular injury induced by electroporation. American Journal of Nuclear Medicine and Molecular Imaging, 2017, 7, 33-39.	1.0	4
41	Targeting of pertechnetate imaging of HepG2 hepatocellular carcinoma through the transduction of the survivin promoter controls the sodium iodide symporter. International Journal of Clinical and Experimental Pathology, 2017, 10, 11037-11043.	0.5	1
42	Selumetinib, an Oral Anti-Neoplastic Drug, May Attenuate Cardiac Hypertrophy via Targeting the ERK Pathway. PLoS ONE, 2016, 11, e0159079.	2.5	20
43	18F-FDG PET/CT for the Diagnosis of Residual or Recurrent Nasopharyngeal Carcinoma After Radiotherapy: A Metaanalysis. Journal of Nuclear Medicine, 2016, 57, 342-347.	5.0	23
44	Biodistribution and evaluation of <sup>131</sup> Iâ€labeled neuropilinâ€binding peptide for targeted tumor imaging. Contrast Media and Molecular Imaging, 2016, 11, 467-474.	0.8	7
45	Fusion to an albumin-binding domain with a high affinity for albumin extends the circulatory half-life and enhances the in vivo antitumor effects of human TRAIL. Journal of Controlled Release, 2016, 228, 96-106.	9.9	64
46	CF750-A33scFv-Fc-Based Optical Imaging of Subcutaneous and Orthotopic Xenografts of GPA33-Positive Colorectal Cancer in Mice. BioMed Research International, 2015, 2015, 1-11.	1.9	7
47	Synthesis and Characterization of Her2-NLP Peptide Conjugates Targeting Circulating Breast Cancer Cells: Cellular Uptake and Localization by Fluorescent Microscopic Imaging. Journal of Fluorescence, 2015, 25, 113-117.	2.5	6
48	Recent Progress of Imaging Agents for Parkinson's Disease. Current Neuropharmacology, 2015, 12, 551-563.	2.9	11
49	Biological Evaluation of <sup>131</sup> I- and CF750-Labeled Dmab(scFv)-Fc Antibodies for Xenograft Imaging of CD25-Positive Tumors. BioMed Research International, 2014, 2014, 1-11.	1.9	13
50	Reduced <sup>64</sup> Cu Uptake and Tumor Growth Inhibition by Knockdown of Human Copper Transporter 1 in Xenograft Mouse Model of Prostate Cancer. Journal of Nuclear Medicine, 2014, 55, 622-628.	5.0	59
51	2-NBDG Fluorescence Imaging of Hypermetabolic Circulating Tumor Cells in Mouse Xenograft model of Breast Cancer. Journal of Fluorescence, 2013, 23, 213-220.	2.5	23
52	Knockdown of copper chaperone antioxidant-1 by RNA interference inhibits copper-stimulated proliferation of non-small cell lung carcinoma cells. Oncology Reports, 2013, 30, 269-275.	2.6	33
53	Bombesin Analogue-Mediated Delivery Preferentially Enhances the Cytotoxicity of a Mitochondria-Disrupting Peptide in Tumor Cells. PLoS ONE, 2013, 8, e57358.	2.5	18
54	Positron Emission Tomography of Human Hepatocellular Carcinoma Xenografts in Mice Using Copper (II)-64 Chloride as a Tracer. Academic Radiology, 2011, 18, 1561-1568.	2.5	29

#	Article	IF	CITATIONS
55	Chondroitin Sulfate as a Molecular Portal That Preferentially Mediates the Apoptotic Killing of Tumor Cells by Penetratin-directed Mitochondria-disrupting Peptides. Journal of Biological Chemistry, 2010, 285, 25666-25676.	3.4	38
56	Selective Apoptotic Killing of Solid and Hematologic Tumor Cells by Bombesin-Targeted Delivery of Mitochondria-Disrupting Peptides. Molecular Pharmaceutics, 2010, 7, 586-596.	4.6	16
57	High-level expression of a functional humanized anti-CTLA4 single-chain variable fragment antibody in Pichia pastoris. Applied Microbiology and Biotechnology, 2009, 82, 41-48.	3.6	15
58	High-level expression of a functional humanized single-chain variable fragment antibody against CD25 in Pichia pastoris. Applied Microbiology and Biotechnology, 2008, 81, 33-41.	3.6	15
59	High level expression of His-tagged colicin 5 in E. coli and characterization of its narrow-spectrum bactericidal activity and pore-forming action. Protein Expression and Purification, 2007, 54, 309-317.	1.3	8